



Hyongsok (Tom) Soh, Ph.D.
University of California
Santa Barbara, CA

Perspectives on Utilizing Unique Features of Microfluidics Technology for Particle and Cell Sorting

Jonathan D. Adams¹ and H. Tom Soh^{2,3*}

¹Department of Physics, University of California, Santa Barbara, CA

²Department of Mechanical Engineering, University of California, Santa Barbara, CA

³Department of Materials, University of California, Santa Barbara, CA

Keywords:

sample preparation, cell sorting, magnetophoresis, microfluidics

Sample preparation is often the most tedious and demanding step in an assay, but it also plays an essential role in determining the quality of results. As biological questions and analytical methods become increasingly sophisticated, there is a rapidly growing need for systems that can reliably and reproducibly separate cells and particles with high purity, throughput, and recovery. Microfluidics technology represents a compelling approach in this regard, allowing precise control of separation forces for high performance separation in inexpensive or even disposable devices. In addition, microfluidics technology enables the fabrication of arrayed and integrated systems that operate either in parallel or in tandem, in a capacity that would be difficult to achieve in macroscale systems. In this report, we use recent examples from our work to illustrate the potential of microfluidic cell- and particle-sorting devices. We demonstrate the potential of chip-based high-gradient magnetophoresis that enable high-purity separation through reversible trapping of target particles paired with high-stringency washing with minimal loss. We also

describe our work in the development of devices that perform simultaneous multitarget sorting, either through precise control of magnetic and fluidic forces or through the integration of multiple actuation forces into a single monolithic device. We believe that such devices may serve as a powerful “front-end” module of highly integrated analytical platforms capable of providing actionable diagnostic information directly from crude, unprocessed samples—the success of such systems may hold the key to advancing point-of-care diagnostics and personalized medicine. (JALA 2009;14:331–40)

INTRODUCTION

Over the past decade, microfluidics technology has come to play an important role in many areas of life sciences and biotechnology¹ ranging from surface plasmon resonance spectroscopy (SPR)² to high-throughput DNA sequencing.³ Because of the well-established advantages offered by microfluidics as a basis for analytical and diagnostic platforms—including minimal use of reagents, low-cost fabrication, functional integration, and disposability—there has been an explosive growth in its use for such applications.⁴ However, microfluidics technology is also proving to be an important asset for particle and cell sorting as a means for sample preparation, a step that is often the most tedious, time-consuming, and perhaps least

*Correspondence: H. Tom Soh, Ph.D., Departments of Materials and Mechanical Engineering, University of California, Santa Barbara, CA 93106, USA; Phone/Fax: +1.805.893.7985; E-mail: tsoh@engineering.ucsb.edu

1535-5535/\$36.00

Copyright © 2009 by The Association for Laboratory Automation
doi:10.1016/j.jala.2009.06.003

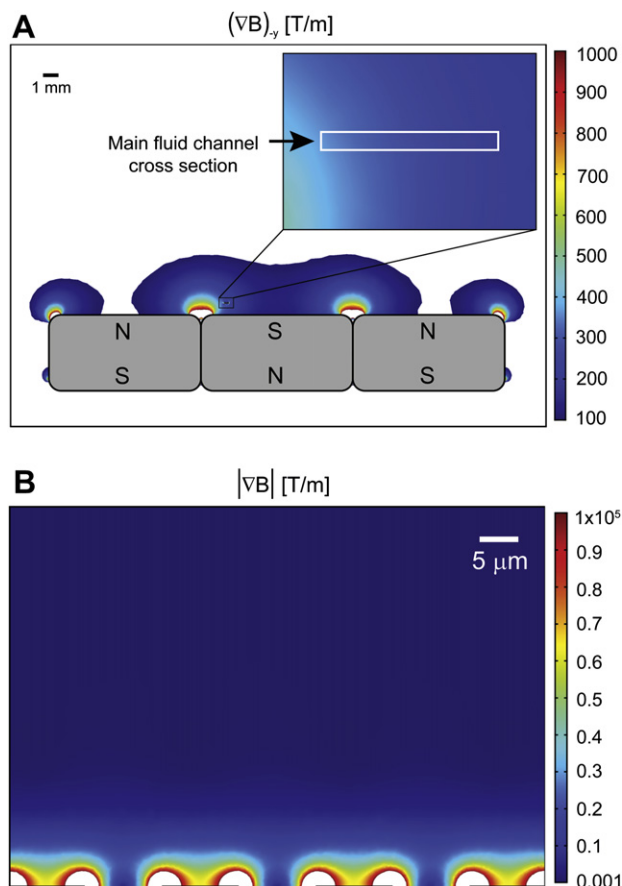


Figure 1. Numerical simulation of long-range and short-range magnetic field gradients in a microfluidic device designed for magnetophoretic separation. (A) Long-range gradients are produced by a series of external permanent magnets, with the magnitude of the $-y$ direction gradient exceeding 200 T/m over the cross section of a microfluidic channel located 0.5 mm above the surface of the magnets. (B) An abrupt change in relative permittivity (μ_r) between microfabricated nickel features ($\mu_r \sim 200$) and the biological sample ($\mu_r \sim 1$) creates an extremely large short-range magnetic field gradient. The magnitude of this gradient is $> 10^4$ T/m within 8 nm of the microfabricated features. Image adapted from Adams et al.³⁵ with permission. © PNAS 2008.

reproducible component of the assay process, yet one which has a critical impact on results.

In general, cell-sorting performance can be benchmarked by three key metrics: purity (the fraction of target cells among collected cells), recovery (the fraction of input target cells successfully collected after sorting), and throughput (number of cells sorted per unit time). Currently, the most widely used methods of cell sorting are magnetically activated cell sorting (MACS) and fluorescence-activated cell sorting (FACS). MACS is a selection technique wherein a magnetically tagged affinity reagent (e.g., antibody) is used to label target cells via a specific surface receptor,^{5–7} enabling labeled cells to be purified from a heterogeneous cell mixture through the application of an external magnetic field gradient. Magnetic selection is thus well

suited for capturing large numbers of target cells in batch mode,⁸ but does not provide analytical information about the purity and recovery of target cells, and this selection method allows only binary selection based on a single parameter (i.e., magnetization). In contrast, FACS is a screening method in which optical signals (e.g., forward/side scatter and fluorescence) detected from a rapidly moving stream of fluorescently labeled cells are measured individually in a cell-by-cell manner, allowing multiparameter separation.⁹ However, due to the serial nature of its operation, FACS offers comparatively low throughput.¹⁰

As biological questions become more complex and cell-based biotechnology applications continue to expand, there is an urgent demand for novel technologies that provide low-cost cell sorting with high purity, recovery, and throughput. For example, some applications of particular interest include purification of scarce populations of stem cells¹¹ and detection of circulating tumor cells.¹² Unfortunately, traditional methods of cell sorting remain limited by the inherent coupling between the competing performance parameters of throughput, purity, and cell recovery. Conceptually, microfluidics provides an alternate strategy for decoupling these parameters through the use of arrayed and integrated devices that can operate both in parallel and in tandem. In addition, microfluidics technology offers unprecedented control over the fluidic and actuation forces that govern the separation process. Finally, chip-based platforms can potentially be made at low cost in a disposable format, reducing the cost per test over complex technologies, such as FACS, and eliminating the risk of cross-contamination between samples. In this report, we will highlight a few examples from our own work that demonstrate how these characteristics can be exploited to achieve novel functionalities and superior cell-sorting performance.

FORCES IN MICROFLUIDIC CHANNELS

Microfluidic devices generally operate within a fluidic regime in which viscous effects are dominant over inertial effects, as characterized by low Reynolds numbers:

$$\text{Re} = \frac{\rho v L}{\eta} \quad (1)$$

where ρ is the fluid density, v is the mean fluid speed, L is a characteristic length, and η is the fluid dynamic viscosity. Thus, fluidic effects on particles are predictable and controllable, and the hydrodynamic drag \vec{F}_d on a particle may be typically described by Stokes' law:

$$\vec{F}_d = 6\pi\eta a(\vec{v}_f - \vec{v}_p) \quad (2)$$

where a is a characteristic length of the particle, v_f the velocity of the fluid, and v_p the velocity of the particle. For spherical particles, a is equal to the radius of the particle; for nonspherical particles, a depends on the particle orientation and must be determined empirically.¹³ The

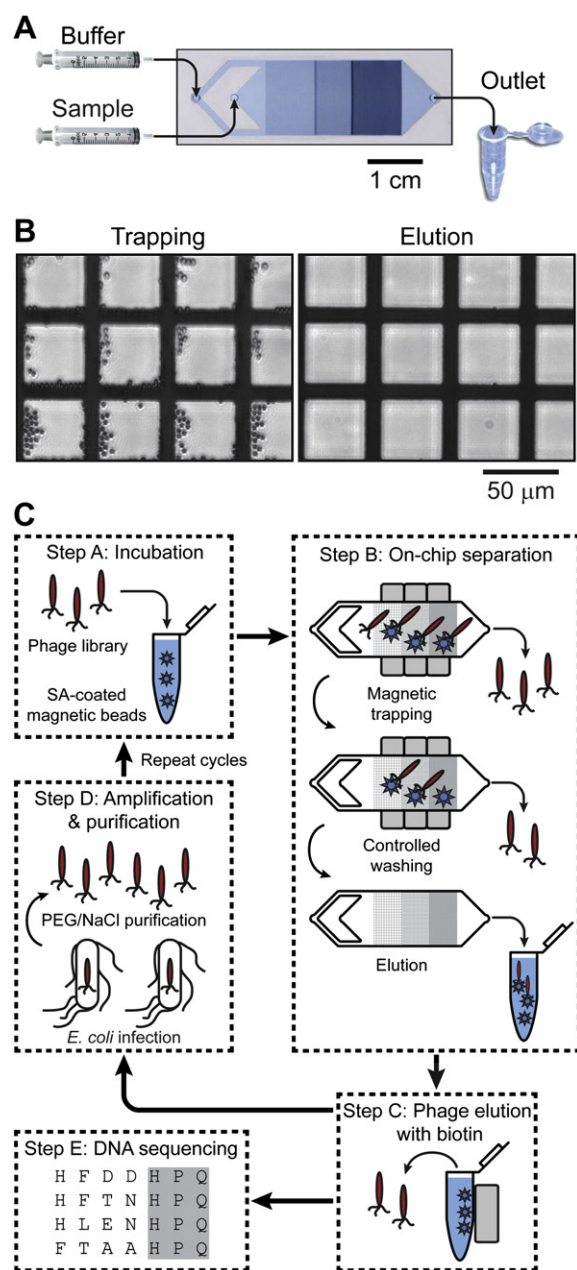


Figure 2. Overview of the Micro-Magnetic Separation (MMS) device and its application for high-purity phage library screening. (A) Micrograph of the MMS device showing the channel design, nickel pattern, and flow path. The device dimensions are 64 mm \times 15.7 mm \times 1.5 mm ($L \times W \times H$), and the height and width of the microfluidic channel are 30 and 12 mm, respectively. (B) Bright field optical micrographs of the nickel pattern in the microchannel. When an external field is applied (left), the large magnetic field gradients at the edges of the nickel pattern effectively trap the beads, but when the external field is removed (right), the nickel pattern is demagnetized and the beads are efficiently eluted. (C) Selection of the phage display library using the MMS device. Step A: The phage library is mixed and incubated with target molecule-conjugated magnetic beads. Step B: neodymium iron boron permanent magnets are applied to the MMS device to

capability to control hydrodynamic forces in microfluidic systems has enabled the development of a number of innovative label-free methods for sorting cells based on inherent physical characteristics such as size, density, and compressibility, including deterministic lateral displacement,¹⁴ pinched flow fractionation,¹⁵ and hydrophoretic filtration.¹⁶

Microfabrication technology has also provided the means for effectively generating a wide variety of force fields within a microchannel, which can be paired with the above-mentioned fluidic forces to perform sophisticated sorting operations that would be difficult to achieve in conventional macroscale systems. Examples include the use of electric fields,^{17–19} magnetic fields,^{20–23} optical fields,^{24–26} and acoustic fields.^{27–30}

Magnetic separation is particularly attractive for biological separations because magnetophoretic forces have minimal effects on cell viability^{31–34} and remain constant over a wide range of environmental conditions (e.g., pH, salinity, and temperature).²² Typically, target cells are magnetically labeled with affinity reagents (e.g., monoclonal antibodies) conjugated to superparamagnetic microparticle or nanoparticle. If superparamagnetic particles are used below saturation, the magnetic force \vec{F}_m may be expressed as:

$$\vec{F}_m = \frac{V_p \Delta \chi}{\mu_0} (\vec{B} \cdot \nabla) \vec{B} \quad (3)$$

where V_p is the particle volume, $\Delta \chi$ is the magnetic susceptibility difference between the particle and the suspension medium, μ_0 is the permeability of free space, and \vec{B} is the magnetic field. For saturated superparamagnetic particles with magnetization m_{sat} oriented along \vec{B} , the magnetic force reduces to a simpler form:

$$\vec{F}_{m,\text{sat}} = m_{\text{sat}} \nabla B \quad (4)$$

Thus, in both cases, accurate generation of magnetophoretic forces requires reproducible generation of magnetic field gradients.

In conventional, large-scale magnetic systems, precision control of magnetic field gradients often requires accurate machining of pole pieces and mechanical alignment.⁸ In contrast, microfabrication technology enables simpler approaches for generating large magnetic field gradients reproducibly,

specifically trap phage particles bound to the magnetic beads, which are subsequently held in place and washed under controlled conditions to eliminate nonspecific interactions. The nickel patterns are then demagnetized, and the phage-carrying beads are eluted. Step C: The phage is dissociated from the protein-conjugated beads by competitive elution with biotin. Step D: Isolated phage is amplified via infection of *Escherichia coli* cells, and subsequently purified with polyethylene glycol/NaCl solution for additional rounds of selection or analysis. Step E: Clones from each round of selection are randomly picked and their DNA is sequenced. Figure reprinted from Liu et al.³⁶ with permission of the authors.

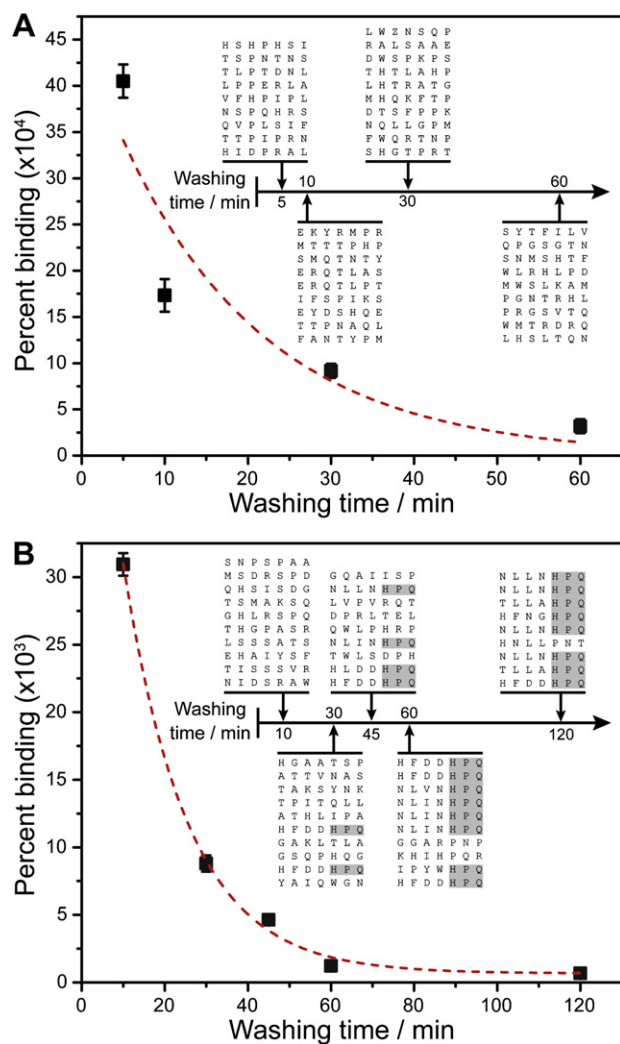


Figure 3. The importance of controlling the washing conditions during phage selection. (A) In the first round of selection, the percentage of recovered phage as a function of washing time decays nonlinearly, as nonspecifically bound and weak binding phage is removed. When modeled as a first-order exponential (dashed line), the dissociation rate constant was $k_{d1} = 1.0 \pm 0.1 \cdot 10^{-3} \text{ s}^{-1}$. (Inset) The canonical target-binding peptide motif (histidine—proline—glutamine [HPQ]) was not found in clones isolated after the first round. (B) In the second round, the percentage of bound phage also showed an exponential decay as stringency (washing time) increased, with a remarkably similar dissociation rate constant of $k_{d2} = 1.07 \pm 0.04 \cdot 10^{-3} \text{ s}^{-1}$. (Inset) The percentage of clones with the HPQ motif increased monotonically as a function of washing time; after 120 min of washing, 8 out of 9 clones contained this motif. Figure reprinted from Liu et al.³⁶ with permission of the authors.

automatically, and inexpensively. For example, recent work by Adams et al.³⁵ demonstrated accurate control over magnetic field gradients within a microfluidic channel over two length scales. Long-range gradients were controlled with a series of external rare-earth (neodymium iron boron) permanent magnets in an alternating configuration (Fig. 1A). These magnets generate $\sim 0.5 \text{ T}$ at their surface and, a gradient of $\sim 200 \text{ T/m}$

in the negative y direction can be generated over the entire cross-sectional area of the microfluidic channel in this configuration. In contrast, short-range gradients were generated by microfabricated ferromagnetic structures (nickel) within the microchannel, as initially described by Inglis et al.²⁰ (Fig. 1B). Here, due to the large difference in relative magnetic permeability between the nickel structures and the biological sample ($\mu_{r,\text{nickel}} = 200$, $\mu_{r,\text{sample}} \sim 1$), the external field reproducibly and accurately induces extremely large short-range gradients ($\sim 10^4 \text{ T/m}$) within $\sim 8 \mu\text{m}$ of the pattern.

MAGNETIC TRAPPING ENABLES STRINGENT WASHING AND HIGH-PURITY SEPARATION

The capability to reproducibly generate large magnetophoretic forces can be combined with stringent, continuous washing within the microchannel to achieve very high purities. To illustrate this point, Liu et al.³⁶ described the Micro-Magnetic Separation (MMS) device for highly efficient screening of phage libraries (Fig. 2A). In this application, a large, diverse library of phage particles displaying unique peptide sequences is screened to specifically isolate clones that bind tightly to a target protein. For assays such as this, high-purity separation is essential.^{37,38}

In the MMS device, target protein—conjugated magnetic beads are trapped by a series of microfabricated ferromagnetic structures embedded within the channel. As described above, the difference in magnetic permeabilities between the sample and the ferromagnetic structures creates high spatial variation in the magnetic field, resulting in a magnetophoretic force of tens of nanonewtons at the edges of the ferromagnetic structures where the gradient is the largest (Fig. 2B, left). Importantly, this trapping is reversible; upon removal of the external field, the ferromagnetic structures demagnetize and the trapped particles are efficiently eluted (Fig. 2B, right). Under experimental conditions, the authors found that 99.5% of the beads that entered the device were successfully trapped, allowing for the use of a small number of beads without significant loss.

The MMS device enables precise control over washing stringency during the phage selection process, as illustrated in Figure 2C. The effects of washing time on the pool of selected peptide sequences were analyzed after two rounds of selection, with the washing flow rate within the chip fixed at 10 mL/h. At this flow rate, the maximum Stokes drag force experienced by the beads was $\sim 10 \text{ pN}$, which was significantly lower than the magnetic trapping force ($\sim 10 \text{ nN}$) and ensured that targets were not eluted inadvertently. The authors observed a nonlinear, inversely proportional relationship between the percentage of bound phage and the washing time, as weakly- or nonbinding phages were progressively removed by longer wash times (Fig. 3A, B). Phage removal over time was modeled as a first-order process, which can be described by simple exponential decay:

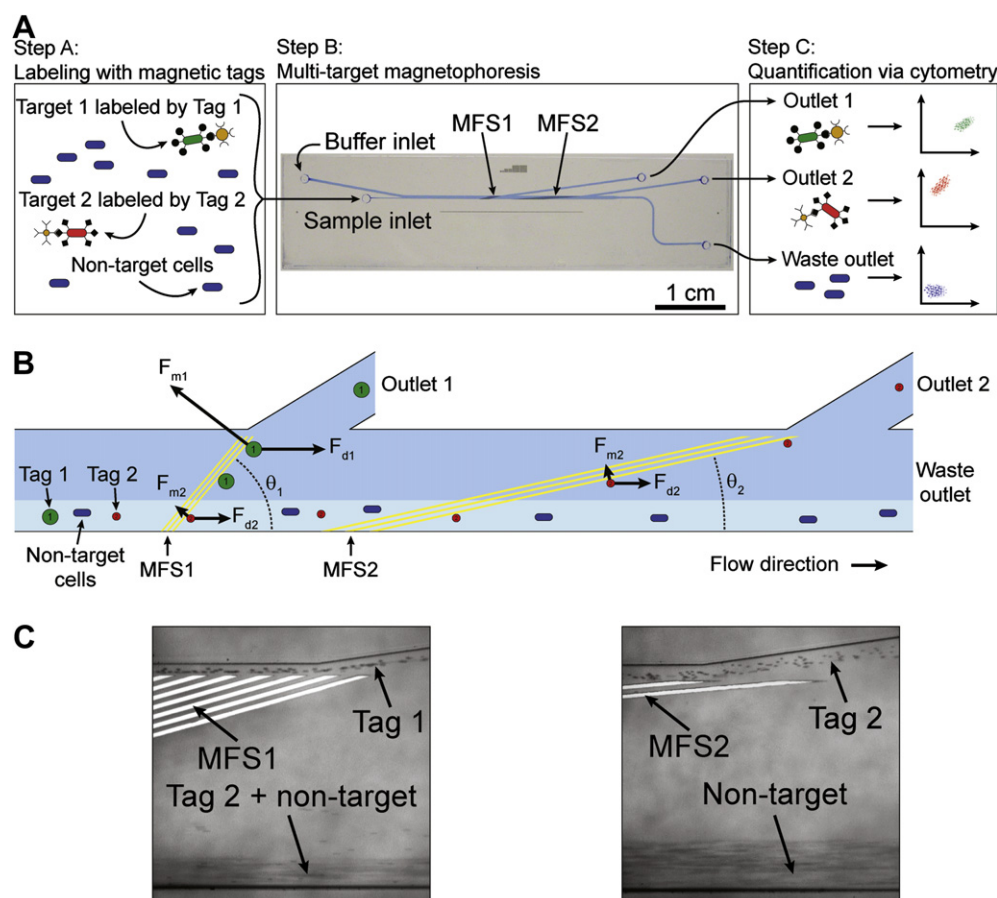


Figure 4. Multi-Target Magnetic Activated Cell Sorter separation architecture. (A) The separation process. Step A: The sample contains an excess of nontarget cells and two different target cell types, which are labeled with two different magnetic tags via specific surface markers. Step B: The sample is continuously pumped into the device, where the two target cell types are sorted into spatially segregated, independent outlets at regions of high magnetic field gradient generated by two sets of microfabricated ferromagnetic strips (MFS 1 and MFS 2). Step C: The eluted fractions from each outlet are analyzed via flow cytometry. (B) A free-body diagram showing the balance of forces at the MFS structures. At MFS 1 ($\theta_1 = 15^\circ$), tag 1-labeled cells are deflected and elute through outlet 1 because $F_{m1} > F_{d1} \sin(\theta_1)$. This is not the case for tag 2-labeled target 2 cells, which are instead deflected at MFS 2 ($\theta_2 = 5^\circ$), where $F_{m2} > F_{d2} \sin(\theta_2)$, and elute through outlet 2. Nontarget cells are not deflected by either MFS and elute through the waste outlet. (C) Optical micrographs (100 \times magnification) of tags being separated at the two MFS structures at a total flow rate of 47 mL/h (sample = 5 mL/h, buffer = 42 mL/h). Tag 1 is deflected at MFS 1 (left), whereas tag 2 is deflected by MFS 2 (right). Figure taken from Adams et al.³⁵ with permission of the authors. © PNAS 2008.

$$S = S_0 e^{-k_d t} \quad (5)$$

where S is the density function at time t for the phage subpopulation remaining bound to the target, S_0 is the amplitude constant, and k_d is the dissociation rate constant.

In this platform, independent and precise control over magnetic trapping forces and washing stringency during phage selection had a direct impact on the effectiveness of the peptide screening process—as washing duration increased, the probability of obtaining consensus peptide sequences increased monotonically (Fig. 3B). After 120 min of washing in the second round, 8 of 9 randomly sequenced clones exhibited the consensus binding sequence histidine–proline–glutamine, compared with only 2 of 10 clones after 30 min of washing. This is one example of how

microfluidics technology can enable extremely high-purity separation in a small sample volume.

ACCURATE CONTROL OF FORCES PERMITS MULTITARGET SEPARATION

In conventional magnetic selection approaches (e.g., tubes and columns), only binary selection is possible because the mechanism of separation is based on a single parameter—the presence or absence of magnetization—and isolation of multiple targets requires multiple stages of purification. However, this is not a fundamental limitation of magnetic separation, and more sophisticated multitarget separation is possible through precise control of magnetic forces. The ability to simultaneously separate multiple target cells via magnetophoresis could reduce both labor time and associated cost per assay

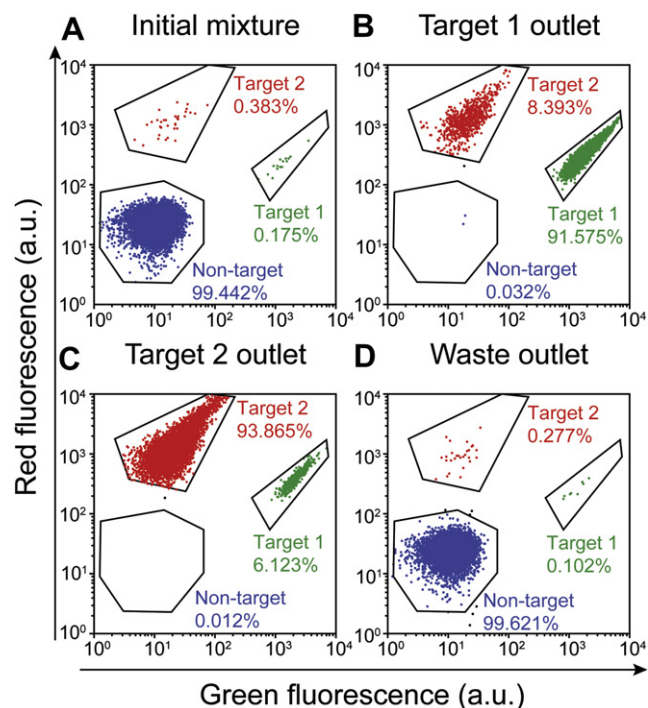


Figure 5. Cytometric analysis of simultaneous, high-purity enrichment of multiple bacterial target cell types in the Multi-Target Magnetic Activated Cell Sorter device. (A) The initial sample mixture consists of 99.442% nontarget cells (expressing blue fluorescent protein) doped with 0.175% target 1 cells and 0.383% target 2 cells. (B) The cell mixture recovered at the target 1 outlet consisted of 91.575% target 1 cells, 8.393% target 2 cells, and 0.032% nontarget cells. (C) The output at the target 2 outlet was composed of 93.865% target 2 cells, 6.123% target 1 cells, and 0.012% nontarget cells. (D) Waste outlet output consisted of 99.621% nontarget cells, 0.102% target 1 cells, and 0.277% target 2 cells. Figure taken from Adams et al.³⁵ with permission of the authors. © PNAS 2008.

compared with conventional magnetic separation, and enable the development of novel purification strategies, such as separation of target cells based on the degree of surface marker expression^{39,40} or magnetic particle uptake.⁴¹

Multitarget magnetic separation has been previously described at the macroscale⁸; however, the generation of large magnetic field gradients in this context is cumbersome, requiring precise positioning of magnets. The generation of such field gradients is greatly simplified in microfluidic systems, however, and we have recently exploited the benefits of working at this scale in the development of their Multi-Target Magnetic Activated Cell Sorter (MT-MACS) chip (Fig. 4).³⁵ The MT-MACS device incorporates multistream laminar flow architecture and microscale magnetic field control for continuous sorting of multiple target cells into independent outlets with high purity and throughput. Here, labeling is performed with two types of affinity reagent-coupled superparamagnetic tags, each with distinct properties of magnetization (M) and radius (r), which specifically bind surface markers expressed by different target cells (Fig. 4A). The labeled sample mixture and running

buffer enter the device through separate inlets; within the device, the balance of the fluidic (F_d) and magnetophoretic (F_m) forces has a nonlinear dependence on the radius, and MT-MACS uses this as a basis to deflect the two types of target cells into two spatially segregated, independent outlets. Briefly, as the cells travel through the device, they encounter two consecutive sets of microfabricated ferromagnetic strips (MFSs), each arranged at different angles (Fig. 4B). The labeled cells are deflected along the MFS if the magnetic force retaining the particle near the MFS edge is greater than the component of the fluidic drag force pulling the labeled cell away from the MFS (i.e., $F_m > F_d \sin(\theta)$). At MFS 1 ($\theta_1 = 15^\circ$), cells labeled with tag 1 (larger in M and r) are deflected because $F_m > F_d \sin(\theta_1)$, whereas cells labeled with tag 2 (smaller in M and r) do not meet this condition and are not deflected. These are instead deflected at MFS 2 ($\theta_2 = 5^\circ$), where $F_m > F_d \sin(\theta_2)$. Unlabeled, nontarget cells are not deflected by either MFS array, and elute through the waste outlet.

The MT-MACS device achieves remarkable enrichment of multiple target cells; working with a mixture of tagged bacterial cells, even low concentrations of labeled target cells ($<0.4\%$) can be simultaneously enriched into highly purified fractions for each target cell type ($>90\%$) in a single pass through the device at a throughput of $\sim 10^9$ cells/h (Fig. 5). This capability to simultaneously separate multiple targets with high purity and throughput could reduce dependence on costly and complex separation procedures, such as FACS. However, the MT-MACS chip is still not capable of true multiparameter separation (i.e., separation based on the presence of two surface markers), and we will review our recent progress toward addressing this technological challenge in the next section.

INTEGRATION OF MULTIPLE SEPARATION FORCES

As a first step toward the goal of integrated multiparameter selection, Kim and Soh⁴² combined multiple separation mechanisms within a monolithic microfluidic device. The integrated Dielectrophoretic-Magnetic Activated Cell Sorter (iDMACS) is a two-input, multiple-output device wherein two types of target cells, labeled with either dielectrophoretic tags (polystyrene microparticles) or magnetic tags (iron oxide-based nanoparticles) are sorted in the presence of an excess background of nontarget cells using two independent force fields (Fig. 6A).

The iDMACS separation is performed in two stages. First, cells are subjected to dielectrophoresis (DEP) forces (F_{DEP}) created by a nonuniform electric field generated by a set of titanium/gold electrodes (Fig. 6B). In this electrode configuration, the F_{DEP} can be described by

$$F_{\text{DEP}} = \frac{27}{32} \pi^2 \epsilon_m \text{Re}(f_{\text{cm}}(\omega)) r^3 \frac{U^2}{a^3} \left[1 + O\left(\frac{r^2}{a^2}\right) \right] \quad (6)$$

where ϵ_m is the permittivity of the medium, r is the distance from the electrode, a is the particle radius, and U is the applied root mean square voltage.¹⁸ $f_{\text{cm}}(\omega)$ is the Clausius–Mosotti

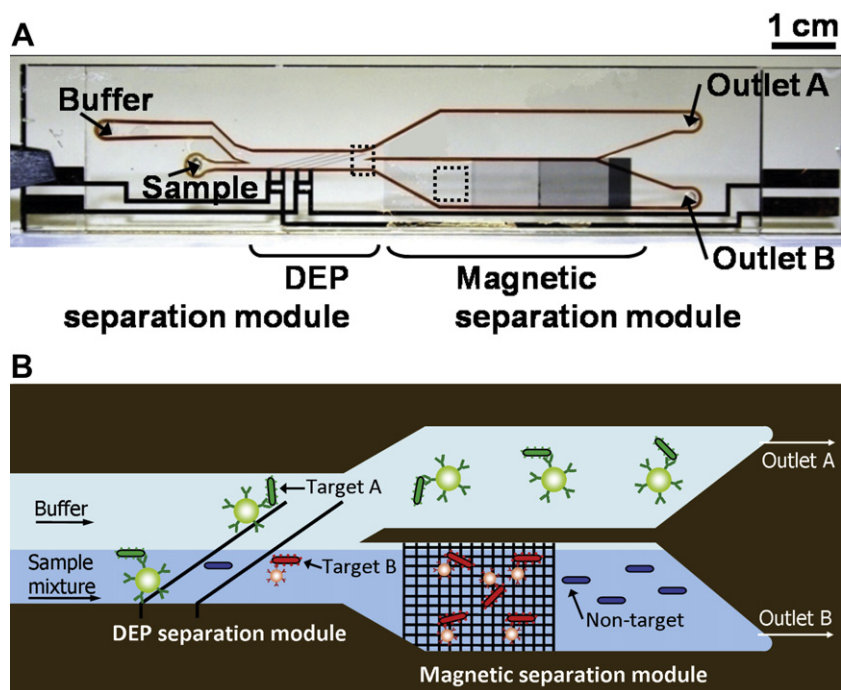


Figure 6. Multitarget bacterial cell sorting via integrated Dielectrophoretic-Magnetic Activated Cell Sorter (iDMACS). (A) Photograph of the fabricated iDMACS device. Overall device size is 7 cm × 1.5 cm, including both dielectrophoresis (DEP) and magnetic separation modules. (B) The physics of multitarget separation via iDMACS. Target A cells, labeled with DEP tags, are deflected at a set of angled electrodes to elute through outlet A. Subsequently, an array of ferromagnetic strips captures magnetically tagged target B cells, which are then eluted through outlet B after washing. Unlabeled nontarget cells are neither deflected by the electrodes nor captured by the strips. Figure reprinted from Kim et al.⁴² with permission of the authors.

factor that describes the competitive polarization between the particle and the suspension medium, given by

$$f_{\text{cm}}(\omega) = \frac{(\epsilon_p^*(\omega) - \epsilon_m^*(\omega))}{(\epsilon_p^*(\omega) + 2\epsilon_m^*(\omega))} \quad (7)$$

where ν_p is the permittivity of the particle and ω is the applied frequency. iDMACS operates in a low-conductivity buffer (0.1 × phosphate buffered saline (PBS), 1% bovine serum albumin (BSA), 20% glycerol), which sets $f_{\text{cm}}(\omega)$ negative; therefore, the overall force is negative and objects are repelled from the electrodes. Here, if the sorting criterion $F_{\text{DEP}} > F_d \sin \theta$ is satisfied,^{43–45} the particle is deflected along the electrodes, redirected into a new flowstream, and eluted through outlet A. Only DEP tag-labeled cells are deflected by the angled electrodes, because they experience F_{DEP} (~2 nN) that exceeds F_{HD} (~0.4 nN) in the direction perpendicular to the electrodes. In contrast, magnetically labeled or unlabeled cells do not meet the DEP sorting criterion, and continue undeflected along the microchannel.

The second stage of interrogation occurs at an array of microfabricated nickel strips (Fig. 6B) that generate high magnetic field gradients as described above. Under standard operating conditions, the magnetic force on labeled cells is estimated to be ~0.3 nN, significantly greater than the fluidic drag force (~0.07 nN), such that magnetically labeled cells are effectively trapped at the nickel strips. As the

magnetic separation component is robust to a wide range of environmental conditions, the same low-conductivity buffer is used throughout the device. After washing, the external magnets are removed and target cells are eluted. A single pass through the iDMACS device yielded up to ~3000-fold enrichment of tags and ~900-fold enrichment of bacterial cells at a throughput of $\sim 2.5 \times 10^7$ cells/h (Fig. 7). Notably, because of the use of two distinct separation forces, there is no crossover contamination between the two target types (i.e., no target A cells in outlet B, and no target B cells in outlet A) in the two enriched populations. Though not shown here, it is certainly possible to combine other separation forces that do not interact with each other (e.g., acoustic, optical, etc.) and such approaches may yield a viable path toward multiparameter selection.

CONCLUSION

In this report, we have highlighted a number of platforms for particle and cell separation that exploit the distinctive features and advantages of microfluidics technology. Using high-gradient magnetophoresis as an example, we have shown that the accurate and reproducible methods of reversibly trapping particles and controlling washing conditions that can be achieved within microchannels enable high-purity separation. We have also shown that the capability to accurately control

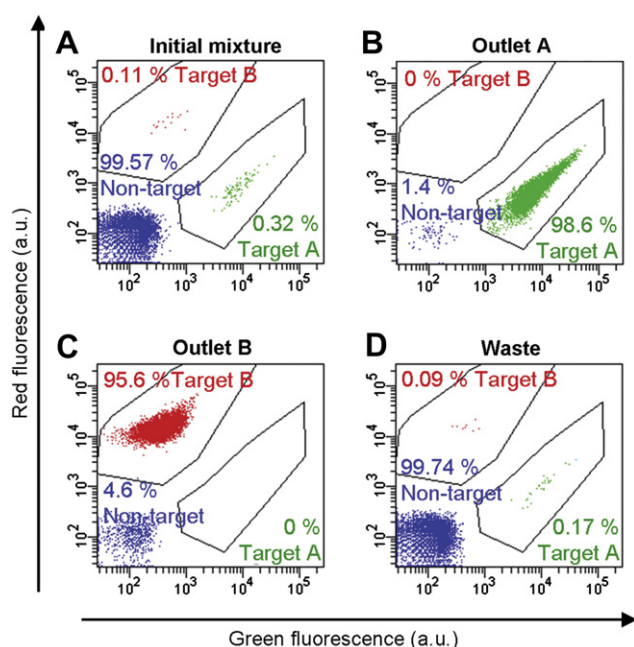


Figure 7. Multitarget bacterial cell-sorting performance using the integrated Dielectrophoretic-Magnetic Activated Cell Sorter device. (A) Two-color flow cytometry measurement of the initial sample, which consisted of an excess of nontarget cells (99.57%) with low concentrations of labeled target A (0.32%) and target B (0.11%) cells. (B) After a single round of separation, the outlet A fraction contained almost exclusively target A cells (98.6%, a 310-fold enrichment), and no target B cells (0%). (C) Conversely, the outlet B fraction contained primarily target B cells (95.6%, a 870-fold enrichment) and no target A cells (0%). (D) The fraction collected at the waste outlet consisted of small quantities of target A (0.17%) and target B (0.09%) cells and mostly nontarget cells (99.74%). Figure reprinted from Kim et al.⁴² with permission of the authors.

both fluidic and magnetic forces enables novel sorting functions, such as simultaneous multitarget selection. Finally, we have noted the benefits of integrating multiple actuation forces into a monolithic device to enable new separation functionalities that would be difficult to implement in conventional macroscale systems. Besides the iDMACS device described here, there are several other examples of platforms that successfully combine forces for multitarget separation. For example, Wiklund et al. effectively combined dielectrophoresis and acoustophoresis,⁴⁶ whereas Liu et al. demonstrated dielectrophoresis with traveling magnetic fields.⁴⁷ In principle, such devices may be operated in parallel to increase throughput^{48,49} or in series to improve purity.⁵⁰

We believe that an important future challenge may lie in the integration of such “front-end” sample preparation techniques with “back-end” analytical methods, and we are beginning to see such integrated systems. For example, Liu et al. have demonstrated a self-contained chip that integrates magnetic capture, PCR amplification, and DNA microarray detection of

bacteria,⁵¹ and more recently, Nagrath et al. combined antibody capture of rare circulating tumor cells in a micropillar array with subsequent on-chip fluorescent detection.⁵² We anticipate that the advent of such highly integrated “sample in-result out” systems⁵³ that can process crude biological samples and yield quantitative, molecular diagnostic information in a disposable format will have a significant impact on many areas of analytical biotechnology, and may hold the key for personalized medicine and point-of-care diagnostics.

ACKNOWLEDGMENTS

We thank the ONR, NIH, ARO Institute for Collaborative Biotechnologies and Armed Forces Institute for Regenerative Medicine for their financial support. We thank Unyoung Kim and Yanli Liu at UCSB, and Andre’ Defusco, Marek Turewicz, Yanting Zhang and Karen Qian at Cynvenio Biosystems (Westlake Village, CA) for their insight and helpful discussions.

REFERENCES

- West, J.; Becker, M.; Tombrink, S.; Manz, A. Micro total analysis systems: latest achievements. *Anal. Chem.* **2008**, *80*(12), 4403–4419.
- Lee, H. J.; Goodrich, T. T.; Corn, R. M. SPR imaging measurements of 1-D and 2-D DNA microarrays created from microfluidic channels on gold thin films. *Anal. Chem.* **2001**, *73*(22), 5525–5531.
- Margulies, M.; Egholm, M.; Altman, W. E.; Attiya, S.; Bader, J. S.; Bembien, L. A.; Berka, J.; Braverman, M. S.; Chen, Y. J.; Chen, Z. T.; Dewell, S. B.; Du, L.; Fierro, J. M.; Gomes, X. V.; Godwin, B. C.; He, W.; Helgesen, S.; Ho, C. H.; Irzyk, G. P.; Jando, S. C.; Alenquer, M. L. I.; Jarvie, T. P.; Jirage, K. B.; Kim, J. B.; Knight, J. R.; Lanza, J. R.; Leamon, J. H.; Lefkowitz, S. M.; Lei, M.; Li, J.; Lohman, K. L.; Lu, H.; Makhijani, V. B.; McDade, K. E.; McKenna, M. P.; Myers, E. W.; Nickerson, E.; Nobile, J. R.; Plant, R.; Puc, B. P.; Ronan, M. T.; Roth, G. T.; Sarkis, G. J.; Simons, J. F.; Simpson, J. W.; Srinivasan, M.; Tartaro, K. R.; Tomasz, A.; Vogt, K. A.; Volkmer, G. A.; Wang, S. H.; Wang, Y.; Weiner, M. P.; Yu, P. G.; Begley, R. F.; Rothberg, J. M. Genome sequencing in microfabricated high-density picolitre reactors. *Nature* **2005**, *437*(7057), 376–380.
- Yager, P.; Edwards, T.; Fu, E.; Helton, K.; Nelson, K.; Tam, M. R.; Weigl, B. H. Microfluidic diagnostic technologies for global public health. *Nature* **2006**, *442*(7101), 412–418.
- Hansel, T. T.; Devries, I. J. M.; Iff, T.; Rihs, S.; Wandzilak, M.; Betz, S.; Blaser, K.; Walker, C. An improved immunomagnetic procedure for the isolation of highly purified human blood eosinophils. *J. Immunol. Methods* **1991**, *145*(1–2), 105–110.
- Miltenyi, S.; Muller, W.; Weichel, W.; Radbruch, A. High-gradient magnetic cell-separation with MACS. *Cytometry* **1990**, *11*(2), 231–238.
- Safarik, I.; Safarikova, M. Use of magnetic techniques for the isolation of cells. *J. Chromatogr. B* **1999**, *722*(1–2), 33–53.
- Chalmers, J. J.; Zborowski, M.; Sun, L. P.; Moore, L. Flow through, immunomagnetic cell separation. *Biotechnol. Prog.* **1998**, *14*(1), 141–148.
- Ashcroft, R. G.; Lopez, P. A. Commercial high speed machines open new opportunities in high throughput flow cytometry (HTFC). *J. Immunol. Methods* **2000**, *243*(1–2), 13–24.
- Ibrahim, S. F.; van den Engh, G. High-speed cell sorting: fundamentals and recent advances. *Curr. Opin. Biotechnol.* **2003**, *14*(1), 5–12.
- Shizuru, J. A.; Negrin, R. S.; Weissman, I. L. Hematopoietic stem and progenitor cells: clinical and preclinical regeneration of the hematolymphoid system. *Annu. Rev. Med.* **2005**, *56*, 509–538.

12. Pantel, K.; Brakenhoff, R. H.; Brandt, B. Detection, clinical relevance and specific biological properties of disseminating tumour cells. *Nat. Rev. Cancer* **2008**, *8*(5), 329–340.
13. Leith, D. Drag on nonspherical objects. *Aerosol Sci. Technol.* **1987**, *6*(2), 153–161.
14. Huang, L. R.; Cox, E. C.; Austin, R. H.; Sturm, J. C. Continuous particle separation through deterministic lateral displacement. *Science* **2004**, *304*(5673), 987–990.
15. Yamada, M.; Nakashima, M.; Seki, M. Pinched flow fractionation: continuous size separation of particles utilizing a laminar flow profile in a pinched microchannel. *Anal. Chem.* **2004**, *76*(18), 5465–5471.
16. Choi, S.; Song, S.; Choi, C.; Park, J. K. Continuous blood cell separation by hydrophoretic filtration. *Lab Chip* **2007**, *7*(11), 1532–1538.
17. Gascoyne, P. R. C.; Vykoukal, J. Particle separation by dielectrophoresis. *Electrophoresis* **2002**, *23*(13), 1973–1983.
18. Durr, M.; Kentsch, J.; Muller, T.; Schnelle, T.; Stelzle, M. Microdevices for manipulation and accumulation of micro- and nanoparticles by dielectrophoresis. *Electrophoresis* **2003**, *24*(4), 722–731.
19. Voldman, J. Electrical forces for microscale cell manipulation. *Annu. Rev. Biomed. Eng.* **2006**, *8*(1), 425–454.
20. Inglis, D. W.; Riehn, R.; Austin, R. H.; Sturm, J. C. Continuous microfluidic immunomagnetic cell separation. *Appl. Phys. Lett.* **2004**, *85*(21), 5093–5095.
21. Pamme, N.; Manz, A. On-chip free-flow magnetophoresis: continuous flow separation of magnetic particles and agglomerates. *Anal. Chem.* **2004**, *76*(24), 7250–7256.
22. Pamme, N. Magnetism and microfluidics. *Lab Chip* **2006**, *6*(1), 24–38.
23. Yellen, B. B.; Erb, R. M.; Son, H. S.; Hewlin, R. Jr.; Shang, H.; Lee, G. U. Traveling wave magnetophoresis for high resolution chip based separations. *Lab Chip* **2007**, *7*(12), 1681–1688.
24. MacDonald, M. P.; Spalding, G. C.; Dholakia, K. Microfluidic sorting in an optical lattice. *Nature* **2003**, *426*(6965), 421–424.
25. MacDonald, M. D.; Neale, S.; Paterson, L.; Richies, A.; Dholakia, K.; Spalding, G. C. Cell cytometry with a light touch: sorting microscopic matter with an optical lattice. *J. Biol. Regul. Homeost. Agents* **2004**, *18*(2), 200–205.
26. Chiou, P. Y.; Ohta, A. T.; Wu, M. C. Massively parallel manipulation of single cells and microparticles using optical images. *Nature* **2005**, *436*(7049), 370–372.
27. Petersson, F.; Aberg, L.; Sward-Nilsson, A. M.; Laurell, T. Free flow acoustophoresis: microfluidic-based mode of particle and cell separation. *Anal. Chem.* **2007**, *79*(14), 5117–5123.
28. Nilsson, A.; Petersson, F.; Jonsson, H.; Laurell, T. Acoustic control of suspended particles in micro fluidic chips. *Lab Chip* **2004**, *4*(2), 131–135.
29. Petersson, F.; Nilsson, A.; Holm, C.; Jonsson, H.; Laurell, T. Separation of lipids from blood utilizing ultrasonic standing waves in microfluidic channels. *Analyst* **2004**, *129*(10), 938–943.
30. Hawkes, J. J.; Barber, R. W.; Emerson, D. R.; Coakley, W. T. Continuous cell washing and mixing driven by an ultrasound standing wave within a microfluidic channel. *Lab Chip* **2004**, *4*(5), 446–452.
31. Gijs, M. A. M. Magnetic bead handling on-chip: new opportunities for analytical applications. *Microfluid. Nanofluid.* **2004**, *1*(1), 22–40.
32. Schenck, J. F. Physical interactions of static magnetic fields with living tissues. *Prog. Biophys. Mol. Biol.* **2005**, *87*(2–3), 185–204.
33. Riviere, C.; Boudghene, F. P.; Gazeau, F.; Roger, J.; Pons, J. N.; Laissy, J. P.; Allaire, E.; Michel, J. B.; Letourneur, D.; Deux, J. F. Iron oxide nanoparticle-labeled rat smooth muscle cells: cardiac MR imaging for cell graft monitoring and quantitation. *Radiology* **2005**, *235*(3), 959–967.
34. Perea, H.; Aigner, J.; Hopfner, U.; Wintermantel, E. Direct magnetic tubular cell seeding: a novel approach for vascular tissue engineering. *Cells Tissues Organs* **2006**, *183*(3), 156–165.
35. Adams, J. D.; Kim, U.; Soh, H. T. Multitarget magnetic activated cell sorter. *Proc. Natl. Acad. Sci. U.S.A.* **2008**, *105*(47), 18165–18170.
36. Liu, Y.; Adams, J. D.; Turner, K.; Cochran, F. V.; Gambhir, S. S.; Soh, H. T. Controlling the selection stringency of phage display using a microfluidic device. *Lab Chip* **2009**, *9*(8), 1033–1036.
37. Lu, D.; Shen, J. Q.; Vil, M. D.; Zhang, H. F.; Jimenez, X.; Bohlen, P.; Witte, L.; Zhu, Z. P. Tailoring in vitro selection for a picomolar affinity human antibody directed against vascular endothelial growth factor receptor 2 for enhanced neutralizing activity. *J. Biol. Chem.* **2003**, *278*(44), 43496–43507.
38. Zhuang, G. Q.; Katakura, Y.; Furuta, T.; Omasa, T.; Kishimoto, M.; Suga, K. A kinetic model for a biopanning process considering antigen desorption and effective antigen concentration on a solid phase. *J. Biosci. Bioeng.* **2001**, *91*(5), 474–481.
39. McCloskey, K. E.; Moore, L. R.; Hoyos, M.; Rodriguez, A.; Chalmers, J. J.; Zborowski, M. Magnetophoretic cell sorting is a function of antibody binding capacity. *Biotechnol. Prog.* **2003**, *19*(3), 899–907.
40. Schneider, T.; Moore, L. R.; Jing, Y.; Haam, S.; Williams, P. S.; Fleischman, A. J.; Roy, S.; Chalmers, J. J.; Zborowski, M. Continuous flow magnetic cell fractionation based on antigen expression level. *J. Biochem. Biophys. Methods* **2006**, *68*(1), 1–21.
41. Pamme, N.; Wilhelm, C. Continuous sorting of magnetic cells via on-chip free-flow magnetophoresis. *Lab Chip* **2006**, *6*(8), 974–980.
42. Kim, U.; Soh, H. T. Simultaneous sorting of multiple bacterial targets using an integrated dielectrophoretic-magnetic activated cell sorter. *Lab Chip* **2009**, in press.
43. Hu, X. Y.; Bessette, P. H.; Qian, J. R.; Meinhart, C. D.; Daugherty, P. S.; Soh, H. T. Marker-specific sorting of rare cells using dielectrophoresis. *Proc. Natl. Acad. Sci. U.S.A.* **2005**, *102*(44), 15757–15761.
44. Kim, U.; Qian, J.; Kenrick, S. A.; Daugherty, P. S.; Soh, H. T. Multitarget dielectrophoresis activated cell sorter. *Anal. Chem.* **2008**, *80*(22), 8656–8661.
45. Kim, U.; Shu, C. W.; Dane, K. Y.; Daugherty, P. S.; Wang, J. Y. J.; Soh, H. T. Selection of mammalian cells based on their cell-cycle phase using dielectrophoresis. *Proc. Natl. Acad. Sci. U.S.A.* **2007**, *104*(52), 20708–20712.
46. Wiklund, M.; Gunther, C.; Lemor, R.; Jager, M.; Fuhr, G.; Hertz, H. M. Ultrasonic standing wave manipulation technology integrated into a dielectrophoretic chip. *Lab Chip* **2006**, *6*(12), 1537–1544.
47. Liu, C. X.; Lagae, L.; Borghs, G. Manipulation of magnetic particles on chip by magnetophoretic actuation and dielectrophoretic levitation. *Appl. Phys. Lett.* **2007**, *90*(18), 184109.
48. Laurell, T.; Petersson, F.; Nilsson, A. Chip integrated strategies for acoustic separation and manipulation of cells and particles. *Chem. Soc. Rev.* **2007**, *36*(3), 492–506.
49. Tan, H. D.; Yeung, E. S. Automation and integration of multiplexed on-line sample preparation with capillary electrophoresis for high-throughput DNA sequencing. *Anal. Chem.* **1998**, *70*(19), 4044–4053.
50. Bessette, P. H.; Hu, X.; Soh, H. T.; Daugherty, P. S. Microfluidic library screening for mapping antibody epitopes. *Anal. Chem.* **2007**, *79*(5), 2174–2178.

51. Liu, R. H.; Yang, J. N.; Lenigk, R.; Bonanno, J.; Grodzinski, P. Self-contained, fully integrated biochip for sample preparation, polymerase chain reaction amplification, and DNA microarray detection. *Anal. Chem.* **2004**, *76*(7), 1824–1831.
52. Nagrath, S.; Sequist, L. V.; Maheswaran, S.; Bell, D. W.; Irimia, D.; Ulkus, L.; Smith, M. R.; Kwak, E. L.; Digumarthy, S.; Muzikansky, A.; Ryan, P.; Balis, U. J.; Tompkins, R. G.; Haber, D. A.; Toner, M. Isolation of rare circulating tumour cells in cancer patients by microchip technology. *Nature* **2007**, *450*(7173), 1235–1239.
53. Easley, C. J.; Karlinsey, J. M.; Bienvenue, J. M.; Legendre, L. A.; Roper, M. G.; Feldman, S. H.; Hughes, M. A.; Hewlett, E. L.; Merkel, T. J.; Ferrance, J. P.; Landers, J. P. A fully integrated microfluidic genetic analysis system with sample-in-answer-out capability. *Proc. Natl. Acad. Sci. U.S.A.* **2006**, *103*(51), 19272–19277.